International Research Journal of Engineering and Technology (IRJET) e-ISSN: 2395-0056
Volume: 09 Issue: 01 | Jan 2022 www.irjet.net p-ISSN: 2395-0072

Indigenously Design Development and Motion Control of Multi-DoF Robotic Manipulator

Muhammad Bilal[1], Muhammad Nadeem Akram[2]

[1]*Human-Centered Robotics Lab, National Centre of Robotics & Automation, University of Engineering & Technology, Lahore-54890, Pakistan*
[2]*Department of Mechanical, Automotive, and Materials Engineering, University of Windsor, Windsor, Ontario, Canada*

Abstract – *A robotic manipulator needs to be compliant, efficient, and lightweight to carry out multiple operations with the desired accuracy in the industrial environment. These factors impose a great challenge to design, analyze, and implementation of control architecture on the sophisticated robotic system. In this pursuit, this study aims to indigenously design and control a six degree of freedom (DOF) robotic manipulator to perform demanded tasks. The mathematical expressions for the robot's motion, including its kinematics and dynamics, have been derived and discussed in detail. Apart from that, the design analysis has been performed to figure out the mechanical system stability. Moreover, the workspace analysis has been carried out followed by a kinematics study using Robotics System Toolbox to ensure the authenticity of derived mathematical models. To validate the forward and inverse kinematics, the position control has been implemented on robotic manipulator hardware using ARM microcontrollers. The robotic manipulator has been controlled through Visual Studio GUI (Graphical User Interface). The transfer function of actual DC motors is estimated using the System Identification Toolbox after needful experimentations. A series of simulations followed by experiments are carried out to effectively validate the design and control architecture. The robot's weight is calculated to be 5.98 Kg with a payload capacity is approximately 330 g. The repeatability test is performed which amounted to ±0.35cm.*

Key Words: Robot design, robot kinematics, position control, pick and place, system identification

1. INTRODUCTION

Nowadays, robots are utilized for multiple tasks, such as painting, polishing, spot welding, pick and place of heavy objects, and many other useful applications [1] [2]. In an industrial environment, robots perform multiple operations with desired accuracy and precision which are unachievable by human workers.

To design a robotic manipulator, first of all, it is required to design a mechanical structure and then model its kinematics [3]. There are multiple fundamental configurations of robotic manipulators available includes articulated, cylindrical, spherical, etc. [4]. These robotic manipulators are used for different kinds of applications as mentioned earlier. As per the design perspective, it is required to select the material which has a high strength to weight ratio to optimize the maximum payload capacity of the robotic manipulator. The lighter the weight of the manipulator the more load it can lift with the assurance of not compromising on material strength.

In terms of the kinematics study, multiple approaches are utilized by researchers, including the screw-based theory [5] and the Denavit-Hartenberg convention [6]. These methods are shown identical results for direct kinematics [7]. The problem of kinematics is divided into two subgroups: 1) Forward Kinematics and 2) Inverse Kinematics [8]. The forward kinematics model of the 6-DoF robotic manipulator is described which is used for different applications [9][10]. Between forward and inverse kinematics, the inverse kinematics is more complex as compared with the forward kinematics [11]. In the last decades, several researchers have worked on the kinematics formulation. For computing the joint variables of a robotic manipulator, a geometric model is presented [12]. The problem of direct kinematics is solved using quaternion algebra [13]. Based on the forward kinematics solution, the inverse kinematics model is presented to solve the joint variables of a serial robotic manipulator [14]. A sophisticated mathematical model of the SCARA robotic arm has been developed with actuator dynamics [15]. The inverse kinematics of the hydraulic arm is computed using MATLAB environment [16]. A virtual robot modal is presented to solve the kinematics problem [17].

The robotic arm has been controlled using an ARM-based microcontroller, LabView, and Dexter ER2 Robotic arm [18]. The joint angles of 5-DoF are calculated and tested using a geometric approach [19]. As per the authors' knowledge, no work has been reported in the past. In this paper, the author presented the kinematics of the 6-DoF robotic arm, including forward and inverse kinematics, with in-depth details to ensure transparency. To validate the kinematics of the manipulator, the model is implemented using a MATLAB environment. The experimental setup to operate 6-DOF robotic manipulator consists of three L298 motor drivers to send PWM and control the direction of actuators. The DC motors with incremental encoders and gear boxes are used as actuators in the robotic manipulator. Furthermore, a

master, and slave topology is employed to ensure the efficient communication and coordination between controllers. A GUI (graphical user interface) is developed to have a user-friendly experience to compute forward, and inverse kinematics. Moreover, a number of repeatability tests are performed to evaluate the precision of manipulator by performing pick, and place task.

The rest of the paper is organized as follows: the mechanical design, robot kinematics and dynamics, DC motor modelling, hardware description, and control scheme are discussed in section 2. After that, the simulations and results are presented in section 3 followed by experiments in section 4. In section 5, the conclusion followed by limitations and future work is presented in section 6.

Figure 1: *Mechanical design of 6-DoF robotic manipulator, including six servo-DC motors, belt-pulley mechanism to enhance torque, control unit, and functional gripper*

2. Methodology

In this subsection, the mechanical design of the 6-DoF robotic manipulator is discussed. The first three joints are in articulated configuration while the last three joints are standard spherical wrist. The mechanical design of the 6-DoF robotic manipulator with timing belt-pulley mechanism and gripper attachment at end-effector is shown in figure 1. In mechanical design, material selection is an important step due to weight, strength, machinability, manufacturability, and assembly easiness. Among the number of materials, aluminum 7075 is chosen based on high strength, less weight, corrosion resistance, and thermal conductivity. More precisely, it has less strength to weight ratio which makes it a better choice for our design. However, this material is expensive, but it has more suitable mechanical properties comparative to 6061 such as its yield strength is 73 kpsi whereas 6061 has just 40 kpsi.

It is not feasible to use a high torque motor without such a mechanism to increase torque. Therefore, timing belt-pulley is employed for motion transmission between motor, and joint shaft. Due to the low load on base, elbow, and wrist as compared to shoulder, GT2 timing belt-pulley with ratio 1:2.08 is employed. While for the shoulder joint, the G3T timing belt-pulley system with a ratio of 1:3.57 is used to effectively hold the shoulder joint at extreme conditions. The thrust bearing is used at the base joint to shift the axial load on the base structure. While the thrust bearing bears axial load but it cannot shift radial load, which is a limitation. On top of that, the thrust bearing provides smooth rotation with negligible friction.

2.2 Position Kinematics

Position kinematics deal with the relationship between joint variables, and task variables of the robotic manipulator. Kinematics plays an important role in a robot's motion. It is further divided into sub-groups: 1) Forward kinematics, and 2) Inverse kinematics.

2.2.1 Forward Kinematics

In forward kinematics, the end-effector variables are calculated for the given pose (position plus orientation). There are two major methods available to calculate the forward kinematics of the n-DOF robotics manipulator: 1) Homogenous transformation and 2) Denavit-Hartenberg (D-H) convention. In the Denavit-Hartenberg convention, there are four parameters used to derive the kinematics model of the robot. Among four parameters, one parameter is variable while the remaining three parameters are constant. According to the D-H convention, the transformation matrix of ith joint w.r.t i-1 joint can be represented as follows:

$$A_i = Rot_{z,\theta} \bullet Trans_{z,d} \bullet Trans_{x,a} \bullet Rot_{x,\alpha} \quad (1)$$

$$T_i^{i-1} = \begin{bmatrix} R_i^{i-1} & P_i^{i-1} \\ \boldsymbol{0} & 1 \end{bmatrix} \quad (2)$$

$$T_i^{i-1} = \begin{bmatrix} c_{\theta i} & -s_{\theta i}c_{\alpha i} & s_{\alpha i}s_{\theta i} & a_i c_{\theta i} \\ s_{\theta i} & c_{\theta i}c_{\alpha i} & -c_{\theta i}s_{\alpha i} & a_i s_{\theta i} \\ 0 & s_{\alpha i} & c_{\alpha i} & d_i \\ 0 & 0 & 0 & 1 \end{bmatrix} \quad (3)$$

Where s_α, s_θ, c_θ and c_α indicate $sin(\alpha)$, $sin(\theta)$, $cos(\theta)$ and $cos(\alpha)$ respectively. While P_i^{i-1} and R_i^{i-1} depict the translation and rotation of *i-1* joint w.r.t *i* joint. The D-H parameters of the 6-DoF robotic manipulator are presented as shown in Table 1. Moreover, the frame of reference on each joint is represented as shown in figure 2. The joint limits are depicted as shown in Table 2. For the given joint variables, the end-effector pose w.r.t world frame for n-DoF can be calculated as follow:

$$T_6^0 = T_1^0 \bullet T_2^1 \ldots T_5^4 \bullet T_6^5 = \begin{bmatrix} R_6^0 & P_6^0 \\ \boldsymbol{0} & 1 \end{bmatrix} \quad (4)$$

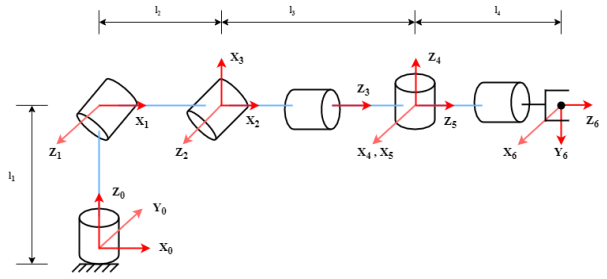

Figure 2: *Frame of Reference on each joint of 6-DoF robotic manipulator based on Denavit-Hartenberg convention to demonstrate the transformation between*

Table 1. *Denavit-Hartenberg parameters of 6-DoF robotic manipulator*

Link No.	*Alpha*	*Link length*	*Joint offset*	*Theta*	*Offset*
1	*pi/2*	*0*	L_1	*	*0*
2	*0*	L_2	*0*	*	*0*
3	*pi/2*	*0*	*0*	*	*pi/2*
4	*pi/2*	*0*	L_3	*	*pi/2*
5	*-pi/2*	*0*	*0*	*	*0*
6	*0*	*0*	L_4	*	*0*

Table 2. *Lower and upper limits of joint variables*

Joint Limits	*Joint variables*					
	Articulated Manipulator			*Spherical Wrist*		
	J1	*J2*	*J3*	*J4*	*J5*	*J6*
Lower (deg)	*-45*	*0*	*0*	*-90*	*-90*	*-90*
Upper (deg)	*45*	*80*	*60*	*90*	*90*	*90*

2.2.1 Inverse Kinematics

In inverse kinematics, the joint variables are calculated for the given end-effector pose. Fortunately, there is one widely used approach available to derive the joint variables expressions in terms of end-effector pose provided the last three joints of robotic manipulator intersecting at a point. In case of 6-DoF robotic manipulator, most robots have decoupled configuration such as three DoF spherical wrist attached with three DoF robot. In such scenario, the inverse kinematics problem is resolved easily by splitting the problem into two subgroups: 1) Inverse position kinematics and 2) Inverse orientation kinematics.

To derive the joint variables expressions for a 6-DoF robotic manipulator, the desired end-effector pose can be expressed as follow:

$$T_6^0 = \begin{bmatrix} r_{11} & r_{12} & r_{13} & x \\ r_{21} & r_{22} & r_{23} & y \\ r_{31} & r_{23} & r_{33} & z \\ 0 & 0 & 0 & 1 \end{bmatrix} \quad (5)$$

Using eq. (5), the wrist center x_c, y_c and z_c can be calculated as:

$$x_c = x - d_6 r_{13} \quad (6)$$

$$y_c = y - d_6 r_{23} \quad (7)$$

$$z_c = z - d_6 r_{33} \quad (8)$$

Where x, y and z depict the end-effector position while d_6 indicate the link length between wrist center and end-effector. Using wrist center, the mathematical expressions for first three joints can be expressed as:

$$\theta_1 = tan^{-1}\left(\frac{y_c}{x_c}\right) \quad (9)$$

$$K = tan^{-1}\left(\frac{z_c - l_1}{\sqrt{x_c^2 + y_c^2}}\right) \quad (10)$$

$$P = cos^{-1}\left(\frac{l_2^2 - l_3^2 + \left(x_c^2 + y_c^2 + z_c^2 + l_1^2 - (2 \times z_c \times l_1)\right)}{2 \times l_2 \times \sqrt{x_c^2 + y_c^2 + z_c^2 + l_1^2 - (2 \times z_c \times l_1)}}\right) \quad (11)$$

$$\theta_2 = K - P \quad (12)$$

$$\theta_3 = tan^{-1}\left(\frac{z_c - l_1 - l_2 \times sin(\theta_2)}{\sqrt{x_c^2 + y_c^2} - cos(\theta_2)}\right) - \theta_2 \quad (13)$$

The term l_1, l_2 and l_3 indicate the base, shoulder, and elbow link lengths, respectively. While θ_1, θ_2 *and* θ_3 represent first, second, and third revolute joints, respectively. Using these joint variables, the remaining spherical wrist angles θ_4, θ_5 *and* θ_6 can be calculated as follow:

$$R_6^0 = R_3^0 \bullet R_6^3 \quad (14)$$

$$R_6^3 = R_3^{0^T} \bullet R_6^0 \quad (15)$$

Where R_6^3 and $R_3^{0^T}$ show rotation of 6th joint w.r.t 3rd joint and rotation of 3rd joint frame w.r.t base joint frame, respectively. By matching R_6^3 with Euler rotation matrix,

$$R_6^3 = \begin{bmatrix} c_4c_5c_6 - s_4s_6 & -c_4c_5c_6 - s_4s_6 & c_4s_5 \\ s_4c_5c_6 + c_4s_6 & -s_4c_5c_6 + c_4s_6 & s_4c_5 \\ -s_5c_6 & s_5c_6 & c_5 \end{bmatrix} \quad (16)$$

The singularity condition is occurred at $\theta_5 = 0$. For nonsingular cases, the following expressions are derived for wrist angles:

$$\theta_4 = atan2\,(r_{23}, r_{13}) \quad (17)$$

$$\theta_5 = atan2\left(\sqrt{1-r_{33}^2}, r_{33}\right) \quad (18)$$

$$\theta_6 = atan2\,(r_{32}, r_{31}) \quad (19)$$

$$\theta_1 = atan2(y_c, x_c) \quad (20)$$

$$var1 = atan\left(\frac{z_c - l_1}{\sqrt{x_c^2 + y_c^2}}\right) \quad (21)$$

$$\text{var2} = \text{acos}\left(\frac{(l_3^2 - l_2^2 - (x_c^2 + y_c^2 + z_c^2 + l_1^2 - (2 * z_c * l_1)))}{-2 * l_2 * \sqrt{x_c^2 + y_c^2 + z_c^2 + l_1^2 - (2 * z_c * l_1)}}\right) \quad (22)$$

$$\theta_2 = var1 - var2 \quad (23)$$

$$\theta_3 = atan2((z_c - l_1 - (l_2 * sin(\theta_2))), \left(\left(\sqrt{x_c^2 + y_c^2}\right) - (l_2 * cos(\theta_2))\right) - \theta_2) \quad (24)$$

Suppose that both r_{13} and r_{23} are zero then,

$$\theta_5 = atan2\left(r_{33}, \sqrt{1 - r_{33}^2}\right) \quad (25)$$

$$\theta_4 = atan2(r_{13}, r_{23}) \quad (26)$$

$$\theta_6 = atan2(-r_{31}, r_{32}) \quad (27)$$

If not both r_{13} and r_{23} are zero, r_{33}>0.999 and $r_{33} < 1.001$ then,

$$\theta_5 = 0 \quad (28)$$

$$\theta_4 = 0 \quad (29)$$

$$\theta_6 = atan2(r_{11}, r_{21}) \quad (30)$$

Otherwise,

$$\theta_4 = atan2(r_{23}, r_{13}) \quad (34)$$

$$\theta_5 = atan2\left(\sqrt{1 - r_{33}^2}, r_{33}\right) \quad (35)$$

$$\theta_6 = atan2(r_{32}, r_{31}) \quad (36)$$

2.3 Robot Dynamics

In robot dynamics, the mathematical expressions indicate the relationship between joint torques and joint accelerations. The inverse dynamics computes the joint torques for the given joint accelerations. While the forward dynamics calculate the joint acceleration for the given joint torques. There are two major methods available to compute the robot dynamics: 1) Newton Euler and 2) Euler-Lagrange. It is not possible to derive the explicit equation of motion with the Newton-Euler formulation. For this reason, the equation of motion is derived using Euler-Lagrange formulation as:

$$\frac{d}{dt}\left(\frac{\partial K}{\partial \dot{q}}\right) - \frac{\partial K}{\partial q} = H\ddot{q} + H\dot{q} - \begin{bmatrix} \dot{q}^T \frac{\partial H}{\partial q_1}\dot{q} \\ \cdot \\ \cdot \\ \cdot \\ \dot{q}^T \frac{\partial H}{\partial q_n}\dot{q} \end{bmatrix} = H\ddot{q} + V(q, \dot{q}) \quad (37)$$

$$H(q)\ddot{q} + C(q, \dot{q})\dot{q} + g(q) + f(\dot{q}) = \tau - J^T F_{ext} \quad (38)$$

where,

$q, \dot{q}, \ddot{q}$ = Joint position, velocity, and acceleration

H(q) = Positive-definite inertial matrix

$g(q)$ = Gravitational forces

$f(\dot{q})$ = Frictional forces

$C(q, \dot{q})\dot{q}$ = Coriolis and centrifugal terms

J = Jacobian matrix

F_{ext} = External forces on end-effector

τ = joint torques

2.4 DC Motor Modelling

To design a PID controller, the transfer function of the motor is required to figure out PID parameters for the given desired transient response. Therefore, the transfer function of the DC motor is identified using System Identification Toolbox in MATLAB. An experiment is performed on each DC motor to compute the input, and output relationship by checking motor RPM with tachometer against multiple input voltages. This data is utilized in the System Identification Toolbox to find a transfer function as shown in figure 3. After that, the PID Tuner App is used for each transfer function to design a robust controller. The PID gains for each DC motor are listed in Table 3.

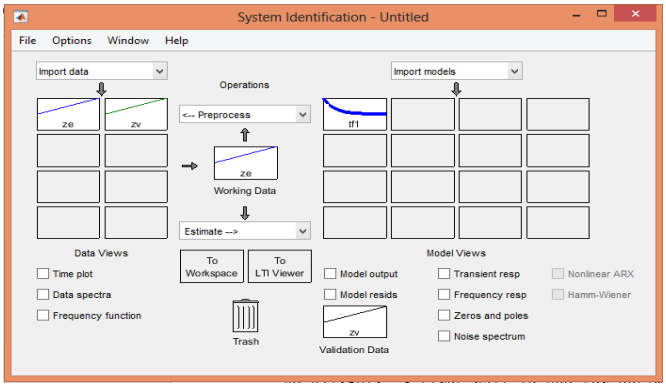

Figure 3: *System identification toolbox for identifying and validating DC motor transfer function*

Table 3: *PID gains of each motor mounted on 6-DoF robotic manipulator*

Motor	*Kp*	*Kd*	*Ki*
Base	100	400	0.00001
Shoulder	120	550	0.00006
Elbow	78	289	0.0009
Wrist 1	144	362	0.008
Wrist 2	206	199	0.0007
Wrist 3	165	183	0.0054

2.5 Hardware Descriptions

2.5.1 Controller

To operate a robotic manipulator, the ARM-based microcontroller Tiva-C tm4c123gxl LaunchPad is employed due to Cortex-M4F 32-bit CPU operating at 80 to 120 MHz. There are two encoder modules available in a single unit. For six actuators, three controllers are used to measure position data from the encoder. The master-slave technique is used for controlling a 6-DoF robotic manipulator.

2.5.2 Actuators

There are several types of actuators available to propel the robotic manipulator, such as electric motors, pneumatics, and hydraulics. Among all types of actuators, electric motors are widely used in robotic manipulators. In this project, encoded DC motors with gearboxes are used for the actuation of the robotic manipulator. A belt-pulley system is used to increase motor torque. To compute the relationship between the motor rotation and link shaft, the following calculation is carried out for the motor mounted on the base joint.

Motor Gear ratio = 43.8:1
Pulley ratio = 2.08:1

To figure out the gear-ratio between shaft and encoder,

$$43.8 \times 2.08 = 91.104$$

After multiplication 91.04 with encoder resolution, the total number of bits are:

$$91.104 \times 32 = 2915.328 \text{ bits}$$
$$360 \text{ degree} = 2915.328 \text{ bits}$$
$$1 \text{ bit} = 360/2915.328 = 0.1234852$$

To compute the exact position/angle of the shaft, this factor will multiply with the current encoder reading. The same calculations are carried out for the remaining five motors as shown in Table 4.

Table 4: *Motor specifications and pre-computation of each motor mounted on 6-DoF robotic manipulator*

Motors	*Gear Ratio*	*Stall Torque (Kg.cm)*	*Stall Current (A)*	*RPM*	*Encoder Res.(CPR)*	*1-bit =*
1st	43.8:1	12	7	251	32	0.1234
2nd	270:1	80	6	40	32	0.0116
3rd	168:1	58	5	80	32	0.0324
4th	131:1	18	5	80	32	0.0858
5th	100:1	16	5	100	32	0.0540
6th	43.8:1	12	7	251	32	0.2568

2.5.3 Sensory System

To ensure mechanical safety, the limit switches are mounted on each joint to stop the manipulator to avoid serious injury. Apart from that, the limit switches are used for detecting home position as a power switch to ON. Moreover, the force sensor is mounted on the end-effector to measure force.

2.6 Control Architecture

In this section, the control scheme is discussed in more detail. To validate the kinematics of the robotic manipulator, the position control scheme is implemented using a PID controller. As mentioned in the previous section, the PID gains are computed based on the estimated transfer function of the DC motor using MATLAB. The PID algorithm can be expressed as:

Current error = desired value - actual value;
*Integral error = (accumulator error) * time period;*
*Derivative error = (Current error – previous error) * 1/time period;*
*PID = kp*Current error + ki*Integral error + kd * Derivative error;*
Previous error = Current error;
Accumulator error += Current error;

3. Results & Discussion

In this section, the simulation studies are discussed in detail to validate the kinematics expressions as well as to explore the workspace of the 6-DoF robotic manipulator. The link lengths are considered to be the unit length of each link. To verify the inverse kinematics formulation, the following 4 by 4 homogenous transformation matrix is given to the robot to compute the joint variables.

$$T_6^0 = \begin{bmatrix} 0.8140 & -0.3642 & 0.4525 & 1.7051 \\ 0.2695 & 0.9269 & 0.2612 & 0.9844 \\ -0.5146 & -0.0907 & 0.8526 & 3.0880 \\ 0 & 0 & 0 & 1.000 \end{bmatrix}$$

For the given pose, the joint variables are computed as presented:

Joint variables (rad) = [0.5233;0.3927;0.6283;1.047;0;0.3490]

To verify the given pose against the computed joint variables, the forward kinematics is implemented to compute the end-effector pose. The results show that the kinematics formulation is accurately derived as shown in figure 4. The calculated 4 by 4 homogenous transformations for the computed joint variables is expressed as:

$$T_6^0 = \begin{bmatrix} -0.6404 & 0.6206 & 0.4525 & 1.7426 \\ -0.5702 & -0.7788 & 0.2612 & 0.9275 \\ 0.5146 & -0.0907 & 0.8526 & 3.0265 \\ 0 & 0 & 0 & 1.000 \end{bmatrix}$$

For the exploration of workspace, the actual link lengths of 6-DoF robotic manipulator are considered as L1 = 13cm, L2 = 13.5cm, and L3 = 38cm. The workspace of the articulated part of the 6-DoF robotic manipulator based on the allowable joint variables range is shown in figure 5.

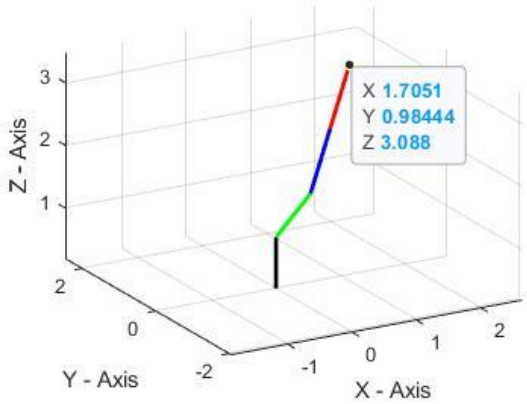

Figure 4: *Implementation of inverse kinematics on 6-DoF robotic manipulator using MATLAB. The end-effector position is represented as highlighted.*

To further verify the kinematics formulation, the circular trajectory is given to the robot with a fixed orientation. In the first case, the link lengths are assumed to be the unit length of each link. The results represented that the robot achieved the desired path with a minute error in the position due to computational error. Figure 6 shows the reference and actual path of the 6-DoF robotic manipulator.

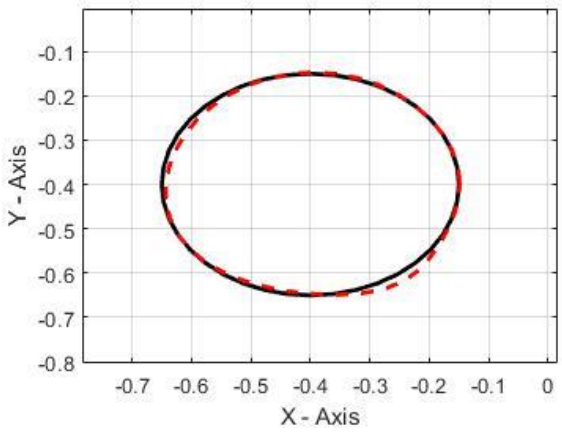

Figure 6: *Circular trajectory tracking. The solid black line indicates the reference path while the dark dashed line depicts the actual path of end-effector*

4. Experiments

After validation of kinematics formulation, the position control using the PID controller is implemented on the hardware. The circuit diagram to control the 6-DoF robotic manipulator is shown in figure 9. There are three controllers used to control six encoded DC motors in which one controller act as a master and the remaining two controllers act as a slave. Moreover, three L298 motor drivers are used to control the PWM and direction of the DC motor. After that, the graphical user interface is designed to get data from the user and actuate the 6-DoF manipulator to achieve the desired pose. Figures 7 and 8 show the layout of the GUI for forward and inverse kinematics. A series of experiments are performed to effectively validate the design structure and control scheme. The joint actions of actual hardware are represented for each joint as shown in figure 10. The repeatability tests are performed which amounted to ±0.35cm. For the pick and place task, the gripper is controlled by a simple servo motor with a force sensor mounted between the jaws of the gripper.

Figure 5: *Workspace analysis of 6-DoF robotic manipulator using MATLAB*

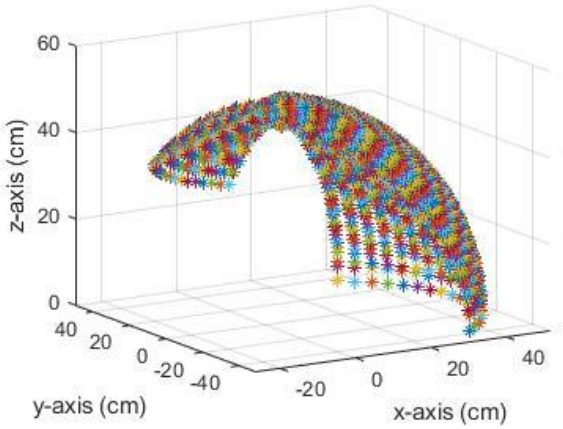

Figure 8: *Forward Kinematics GUI layout to control*

5. Conclusions

In this study, the authors design, analyze, and fabricate the 6-DoF robotic manipulator for pick and place operation. Moreover, the position control is implemented using an ARM-based microcontroller to effectively validate the robot kinematics, including forward and inverse kinematics. The mathematical expressions for robot kinematics are derived and elaborated in more detail. The transfer function of the DC motor is estimated using the System Identification Toolbox after collecting motor RPM data by applying a series of input voltages. To control a robotic manipulator, the graphical user interface is developed using Visual Studio. The robot payload capacity is amounted to 330g while the robot's weight is 5.98 Kg. A number of experiments performed to test the repeatability of the robot which came out ±0.35cm. The force sensor is employed on the end-effector to measure gripping force.

Figure 7: *Inverse kinematics GUI layout to control the*

6. Limitations and Future Work

On the off chance that you have 6 DOF, a given end-effector present is just reachable in a specific configuration of the robot. Unless provided that you have extra joints, you can in any case move the arm without moving the end-effector so that for instance the elbow of the arm isn't slamming into parts of the workspace. So, a 7-DOF redundant manipulator will be used to reach the unreachable points of the work envelope. In the upcoming versions of our robot, we will ensure cylindrical links have an even load distribution in our design and improved aesthetics as well. The replacement of Brushed DC motors with Brushless DC motors will give us more control and precision to achieve our desired position and trajectory. Above all that high resolution incremental optical encoders or absolute encoders would contribute to more

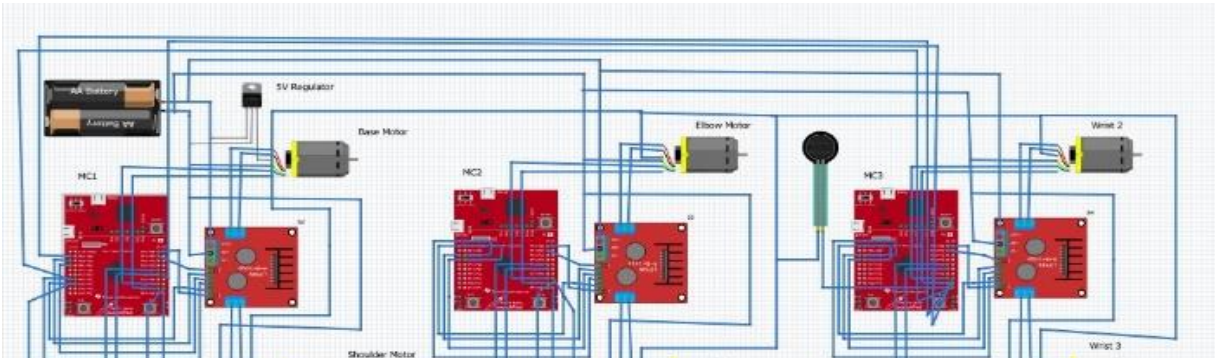

Figure 9: *Circuit diagram to control a 6-DoF robotic manipulator, including six DC servo motors, three motor drivers, three ARM microcontrollers, power supply, and force sensor mounted on end-effector*

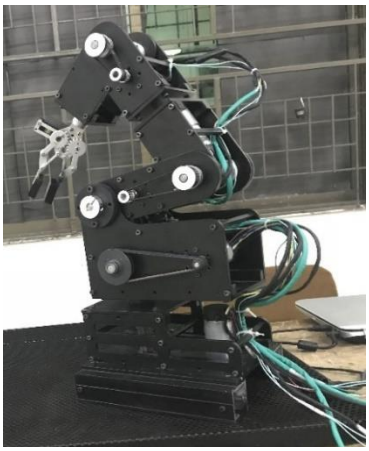
Home position

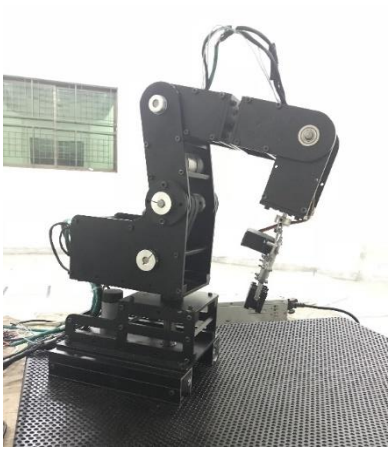
Shoulder joint 60 degree


Elbow joint 45 degree


1st wrist motor 45 degree


Second wrist motor 45 degree


Third wrist motor 45 degree

Figure 10: *Experimentations on 6-DoF robotic manipulator to ensure the validity of forward and inverse kinematics.*

precise feedback in a closed-loop system. If we have enough cost for manufacturing, we can use Aluminum 7075-T6 instead of 6061-T6 to have more strength to weight ratio.

References

[1] J. Liu and Q. Luo, "Modeling and Simulation of Robotic Arm in MATLAB for Industrial Applications," Proc. - 2019 11th Int. Conf. Intell. Human-Machine Syst. Cybern. IHMSC 2019, vol. 1, pp. 346–349, 2019, doi: 10.1109/IHMSC.2019.00086.

[2] M. Dahari and J. D. Tan, "Forward and inverse kinematics model for robotic welding process using KR-16KS KUKA robot," 2011, doi: 10.1109/ICMSAO.2011.5775598.

[3] E. ELIOT, B. B. V. L. DEEPAK, D. R. PARHI, and J. SRINIVAS, "DESIGN & KINEMATIC ANALYSIS OF AN ARTICULATED ROBOTIC MANIPULATOR," Int. J. Mech. Ind. Eng., pp. 12–15, 2014, doi: 10.47893/ijmie.2014.1177.

[4] S. Küçük and Z. Bingül, "The inverse kinematics solutions of industrial robot manipulators," in Proceedings of the IEEE International Conference on Mechatronics 2004, ICM'04, 2004, pp. 274–279, doi: 10.1109/icmech.2004.1364451.

[5] S. A. Ajwad, M. I. Ullah, R. U. Islam, and J. Iqbal, "Modeling Robotic Arms – A Review and Derivation of Screw Theory Based Kinematics," no. January, 2014, [Online]. Available: https://192.169.156.207/wp-content/uploads/2017/04/19-1.pdf.

[6] H. Lipkin, "A note on Denavit-Hartenberg notation in robotics," in Proceedings of the ASME International Design Engineering Technical Conferences and Computers and Information in Engineering Conference - DETC2005, 2005, vol. 7 B, pp. 921–926, doi: 10.1115/detc2005-85460.

[7] A. A. Mohammed and M. Sunar, "Kinematics modeling of a 4-DOF robotic arm," in Proceedings - 2015 International Conference on Control, Automation and Robotics, ICCAR 2015, 2015, pp. 87–91, doi: 10.1109/ICCAR.2015.7166008.

[8] T. P. Singh, P. Suresh, and S. Chandan, "Forward and Inverse Kinematic Analysis of Robotic Manipulators," Int. Res. J. Eng. Technol., vol. 4, no. 2, pp. 1459–1469, 2017, Accessed: Nov. 28, 2021. [Online]. Available: https://www.academia.edu/download/52018593/IRJET-V4I2286.pdf.

[9] A. Khan and W. L. Quan, "Forward kinematic modeling and analysis of 6-DOF underwater manipulator," Proc. 2015 Int. Conf. Fluid Power Mechatronics, FPM 2015, pp. 1093–1096, 2015, doi: 10.1109/FPM.2015.7337281.

[10] N. Panigrahi and K. K. Dash, "Kinematic Model Design of a 6 DOF Industrial Robot," in Applications of Robotics in Industry Using Advanced Mechanisms, 2020, pp. 203–212.

[11] M. W. Spong, S. Hutchinson, and M. Vidyasagar, "Robot modeling and control," IEEE Control Systems, vol. 26, no. 6. pp. 113–115, 2006, doi: 10.1109/MCS.2006.252815.

[12] K. E. Clothier and Y. Shang, "A Geometric Approach for Robotic Arm Kinematics with Hardware Design, Electrical Design, and Implementation," J. Robot., vol. 2010, pp. 1–10, 2010, doi: 10.1155/2010/984823.

[13] S. Sahu, B. B. Biswal, and B. Subudhi, "A Novel Method for Representing Robot Kinematics using Quaternion Theory," IEEE Spons. Conf. Comput. Intell. Control Comput. Vis. Robot. Autom., pp. 76–82, 2008, Accessed: Nov. 28, 2021. [Online]. Available: http://dspace.nitrkl.ac.in/dspace/handle/2080/689.

[14] S. N. Cubero, "Blind search inverse kinematics for controlling all types of serial-link robot arms," in Mechatronics and Machine Vision in Practice, Springer Berlin Heidelberg, 2008, pp. 229–244.

[15] M. T. Das and L. C. Dülger, "Mathematical modelling, simulation and experimental verification of a scara robot," Simul. Model. Pract. Theory, vol. 13, no. 3, pp. 257–271, 2005, doi: 10.1016/j.simpat.2004.11.004.

[16] K. Kong and M. Tomizuka, "Control of exoskeletons inspired by fictitious gain in human model," IEEE/ASME Trans. Mechatronics, vol. 14, no. 6, pp. 689–698, 2009, doi: 10.1109/TMECH.2009.2032685.

[17] R. Kumar, P. Kalra, and N. R. Prakash, "A virtual RV-M1 robot system," Robot. Comput. Integr. Manuf., vol. 27, no. 6, pp. 994–1000, 2011, doi: 10.1016/j.rcim.2011.05.003.

[18] C. C. Mouli, "Design and Implementation of Robot Arm Control Using LabVIEW and ARM Controller," IOSR J. Electr. Electron. Eng., vol. 6, no. 5, pp. 80–84, 2013, doi: 10.9790/1676-0658084.

[19] K. E. Clothier and Y. Shang, "A Geometric Approach for Robotic Arm Kinematics with Hardware Design, Electrical Design, and Implementation," J. Robot., vol. 2010, pp. 1–10, 2010, doi: 10.1155/2010/984823.